

Article

Interaction of Irregular Distribution of Submerged Rigid Vegetation and Flow within a Straight Pool

Kourosh Nosrati ¹, Hossein Afzalimehr ^{1,*} and Jueyi Sui ²

¹ Natural Disasters Prevention Research Center, Faculty of Civil Engineering, Iran University of Science and Technology, Tehran 16846-13114, Iran; koursoh_nosrati@civileng.iust.ac.ir

² School of Engineering, University of Northern British Columbia, Prince George, BC V2N 4Z9, Canada; jueyi.sui@unbc.ca

* Correspondence: hafzali@iust.ac.ir; Tel.: +98-913-2175524

Abstract: The interaction of bedform and vegetation cover significantly affects the turbulent flow parameters. To investigate this interaction, experiments were carried out in both a gravel-bed river and a laboratory flume. The purpose of field investigations was to find the slopes for both the entrance section and exit section of pools, the grain size of the bed material, and the flow condition. Based on field data, without considering any scaling analysis, a straight pool was constructed in a laboratory flume that was 0.9 m wide, 0.6 m deep, and 14 m long. The entry and exit slopes of the straight pool were 7.4° and 4°, respectively. The straight pool had vertical side walls and a gravel bed with a median grain size of $d_{50} = 23.3$ mm. Plastic cylinders planted in an irregular pattern in the channel beds were used to model rigid submerged vegetation. The velocity components were recorded by using an ADV at 200 Hz. In this study, the distributions of velocity, Reynolds stress, and TKE were investigated for flows in the presence of submerged rigid vegetation in channel beds with various area densities of vegetation. Results show that the shape of Reynolds stress distribution depends on the entrance and exit slopes of the pool, as well as the irregular distribution pattern of vegetated elements. Inside the pool with the presence of submerged vegetation in the channel bed, the maximum TKE appears above the bed surface with a larger distance depending on the area density of vegetation in the channel bed. However, the momentum exchange and turbulent energy are likely influenced by the secondary circulation of the flows associated with the irregular distribution of vegetated elements in the channel bed. Results of the quadrant analysis show that the momentum between the flow, bedform, and vegetated elements is mostly transferred by sweep and ejection events. The outward event tends to grow toward the water surface, reaching the highest amount near the water surface. At the pool entrance section where the flow is decelerating, the ejection event is dominant near the bed while the sweep event is strong near the water surface. With the decrease in the vegetation density in the pool bed, both the ejection and outward events become dominant.

Keywords: submerged rigid vegetation; 3D bedform; Reynolds stress; quadrant analysis



Citation: Nosrati, K.; Afzalimehr, H.; Sui, J. Interaction of Irregular Distribution of Submerged Rigid Vegetation and Flow within a Straight Pool. *Water* **2022**, *14*, 2036. <https://doi.org/10.3390/w14132036>

Academic Editors: Anargiros I. Delis and Giuseppe Pezzinga

Received: 4 April 2022

Accepted: 21 June 2022

Published: 25 June 2022

Publisher's Note: MDPI stays neutral with regard to jurisdictional claims in published maps and institutional affiliations.



Copyright: © 2022 by the authors. Licensee MDPI, Basel, Switzerland. This article is an open access article distributed under the terms and conditions of the Creative Commons Attribution (CC BY) license (<https://creativecommons.org/licenses/by/4.0/>).

1. Introduction

Vegetation in channel beds and river banks plays a very important role in aquatic systems and benefits the river environment by improving the river water quality by producing oxygen [1], preventing river bank erosion [2], and providing appropriate habitat diversity for fish [3]. Physically, the presence of vegetation patches in rivers modifies the velocity profiles resulting in either positive responses, such as the accumulation of nutrients due to the stress reduction, or negative responses, such as the depletion of nutrients due to the stress enhancement [4].

The effect of vegetation on the velocity profile and turbulence characteristics depends on the type of vegetation (rigid or flexible) and the flow conditions around the vegetation (submerged or emergent). Significant research has been conducted to study the interaction

between hydrodynamics and vegetation in recent years [5–9]. Flume experiments have been carried out by using natural vegetation [10–12] or simple elements such as strips or cylinders [13,14]. Field measurements of flow have also been conducted in natural rivers in the presence of submerged vegetation [15–17]. Many theoretical and numerical investigations have been performed, focusing mainly on the evaluation of velocity, shear stress, and turbulence intensity distributions [8,18,19]. For submerged vegetation in channels, Baptist et al. (2007) pointed out that there are four distinct zones in the vertical velocity profile, although the velocity profile is often described by two interacting zones, known as the two-layer approach, namely, the vegetation layer which contains cylindrical elements known as vegetation, and the surface layer above the vegetation (up to the water surface) [20].

For vegetation with the same arrangement pattern and the same height, the characteristics of flow within a group of submerged cylindrical elements are similar to those in the case of emergent vegetation [21]. Above the cylindrical vegetated elements, the flow velocity moves to a higher inflection point. The two co-flowing streams (the upper one and the one between the vegetal elements) increase to generate a Kelvin–Helmholtz instability, which causes the flow to rotate clockwise, and vortices to become larger in the downstream direction, forcing the inflection point to locate in the vegetal zone. For sparse vegetation, the vortex affects the whole vegetated layer, whereas, in the case of dense vegetation, it affects only a layer confined to the top of the vegetated elements [7]. The longitudinal turbulence intensities reach a maximum near the top of the vegetated elements. It has the largest values behind the vegetated elements and decreases in the flow direction. In the free stream region, the longitudinal turbulence intensity reaches the lowest value.

Rigid submerged vegetation in channel beds has attracted the attention of quite a few researchers [7,18,20,22–25]. Some researchers provided the average velocity values in the two layers, while others derived the velocity distribution [7,24]. In the vegetated layer, the streamwise velocity is usually considered constant over the layer depth [13,24], while in the surface layer, various expressions were adopted for the velocity distribution [26], namely, the logarithmic theory [22], the Kolmogorov theory of turbulence [27], the genetic programming [20], and the representative roughness height [28]. Nikora et al. (2013) reported that the flows can be divided into five sub-layers: bed-boundary, uniform, mixing, logarithmic, and wake layers [29]. The bed-boundary layer is usually very thin. The velocity in this layer rapidly increases with the distance from the channel bed. In the uniform layer, the drag force is balanced by the sliding force, causing a relatively uniform velocity distribution. The mixing layer is the most complicated and can be described by a hyperbolic tangent profile [7]. In the logarithmic layer, the velocity follows the law of the wall. In the wake layer, the velocity profile should be modified with a wake term. However, this kind of velocity distribution is complex and hardly occurs in practice. The resistance resulting from vegetated elements reduces the velocity within the canopy of vegetation compared to the overflow, such that the canopy of vegetation interface is a region with strong shear resembling a free-shear layer [30]. Raupach et al. (1996) demonstrated the analogy between terrestrial canopy-shear-layers and free-shear-layers, which includes similarity in the scaling of both mean flow and turbulent statistics [31]. This kind of analogy can be extended to aquatic vegetation [32]. It is important to note that a shear layer is generated only when the momentum absorption by the vegetation canopy is sufficient to produce an inflection point in the velocity profile, which needs to trigger the Kelvin–Helmholtz instability. The turbulent flow type in the horizontal-vertical plan varies with an increase in the area density of vegetation, from the bed-shear flow to the free-shear flow [33]. The bed-shear flow happens because of bed drag near the channel bed, and the presence of vegetation contributes to the bed roughness and increases the bed friction. For the medium dense distribution of vegetation, the flow discontinuity caused by the drag of the vegetation canopy would occur at the top of the vegetation, generating the free-shear flow in a certain vertical region [34].

There are some models proposed to consider the effect of vegetation on flow resistance [24,28]. These models are mostly restricted to vegetated elements with specific

arrangements and morphology in channel bed, and thus, they are not easily applied to other vegetation species or morphologies. For example, Yang and Choi (2010) proposed a two-layer model where the momentum balance was applied to each layer and an expression for the mean velocities was proposed. The flow velocity was assumed uniform in the vegetation layer and logarithmic in the upper layer [24]. Cheng (2011) proposed a representative roughness height to describe the resistance caused by vegetation in open-channel flows. He pointed out that the friction factor determined for the surface layer above the vegetation normally increases with the relative roughness (d_{50}/H) [28]. Therefore, the flow characteristics for submerged rigid vegetation should be analyzed to reveal general reasonable results based on laboratory data.

However, to the best of our knowledge, the interaction between randomly vegetal elements and 3D bedforms over a range of vegetation area densities has not been reported. The longitudinal profiles of various gravel-bed rivers are defined as the changes in topographic highs and lows describing macroscale bedforms such as pools and riffles. Pools and riffles are geomorphological features often found in straight, meandering, and braiding river systems [35]. They have been considered essential elements for initiating and developing river bends [36]. Recently, it has been realized that the hydrodynamic variability of the pools-riffles cascade provides a variety of habitat conditions required for different fish species and the same species at different stages of its life [37].

It is well understood that the characteristics of velocity and Reynolds stress distributions depend on a balance between the accelerating force of gravity and the resistance (channel bed and walls) in a uniform flow. In a pool, the flow depth will first increase and then decrease, which inevitably results in a decelerating flow (DF) and an adverse pressure gradient in the streamwise direction, followed by an accelerating flow (AF) and a favorable pressure gradient. The inertial effects say that in the outer flow zone (farther from the bed), streamwise velocity remains relatively high in the DF and relatively low in the AF [38]. The vegetation cover in the channel bed significantly affects the concentration of the suspended load, oxygen level, and water quality. However, the interaction of vegetation and bedforms is an important factor in river morpho-dynamics. In recent decades, many field and laboratory studies have been conducted to investigate the effect of vegetation on flow hydrodynamics in the presence of bedforms [6,39,40], and also periodic beds [41,42]. For example, in a flume with vegetated walls, Nasiri et al. (2011) found that the Reynolds stress at downstream and upstream locations of a gravel bedform has a convex distribution profile.

To the best of our knowledge, the impact of the irregular distributions of vegetated patches on the characteristics of turbulent flow in the presence of 3D bedforms has hardly been studied. The objectives of the present study are, therefore, to investigate the following questions:

How do the velocity, Reynolds stresses, and turbulence kinetic energy change with the irregularity of vegetation cover over an artificial 3D pool? What are the dominant events in the bursting process when the submerged vegetation is distributed irregularly over a pool?

To answer these questions, laboratory experiments have been conducted in a straight, artificial pool with the presence of submerged rigid vegetation patches with various irregular distribution patterns. Laboratory results were compared to those of a natural gravel river in central Iran which has a similar flow depth, vegetation cover, and grain size.

2. Materials and Methods

Experiments were carried out in both a natural river and a laboratory flume. The purpose of field investigations in a natural river was to find the slopes for both the entrance section and exit section of pools in a gravel-bed river, grain size of bed material, and flow condition. Based on the data collected in the natural gravel-bed river, a pool was constructed in a laboratory flume without conducting any dimensional analysis and scaling. The pool in the laboratory flume had approximately similar conditions to those of the gravel-bed river, including morphology, grain size, and flow depth.

2.1. The Field Study

The Marbor Padena River is located in the south of Isfahan Province in central Iran. The study site was a straight gravel-bed reach. Figure 1 shows the location of the study river reach where a pool with irregular submerged vegetation is prevalent.

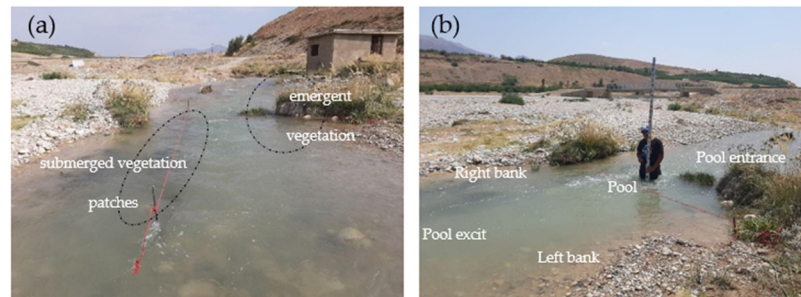


Figure 1. (a) Location of the selected reach in the Padena Marbor River; (b) topographic surveying.

The geometric dimensions of this pool were determined based on the topographic survey along the selected river reach which is 8.5 m long. The average width of this reach is 4.4 m, with the entrance and exit slopes of 7.4 degrees and 4 degrees, respectively. The flow depth H at the centerline of the pool entrance was 0.45 m, measured with a ruler with an accuracy of 1 mm. The flow velocity was also measured using a Butterfly Current Meter with an accuracy of 0.1 m/s. The time of velocity recordings at each point was 50 s, and the measurements at each point were repeated three times. The flow rate Q was calculated by using the continuity equation $Q = \sum_{i=1}^n u_i A_i$ where A_i is the area of each sub-cross-section and u_i is the mean velocity in each sub-cross-section. At the pool entrance, the discharge was $Q = 1.79 \text{ m}^3/\text{s}$, the average flow velocity $U = 1.0 \text{ m/s}$, the Reynolds number $Re = UH/\nu_m = 424,620$, and the Froud number $Fr = U/(gH)^{0.5} = 0.5$. The values of Re and Fr indicate a fully turbulent and sub-critical flow at the pool entrance.

Figure 2 presents the grain size distribution of bed material in both the selected pool in the river and the artificial pool in the flume, obtained by using the Wolman technique [41]. In fact, gradings were done at the pool entrance, in the pool, and the pool exit for surface layers (as the upper limit of grading) and the lower layer (as the lower limit of grading). The grading used in the laboratory study is the middle one of these grain size distributions. The median grain size of the bed material in the field study ranged from 9.2 mm to 23.4 mm with the geometric standard deviation ($\sigma_g = (d_{84}/d_{16})^{0.5} = 2.63$, where, d_{84} and d_{16} are 16th and 84th percentile of the particle-size distribution, respectively, and show the grain size distribution is non-monotonous [17].

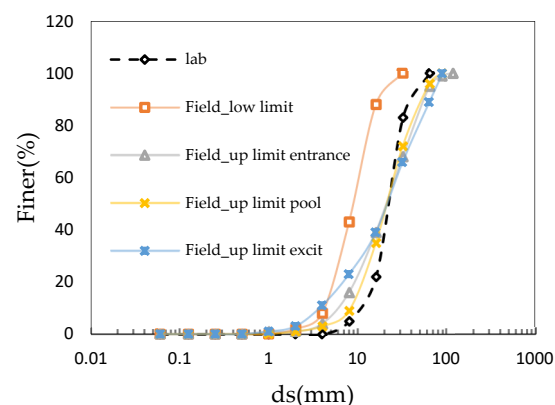


Figure 2. The grain size distribution of bed material in the river and flume.

2.2. Experimental Study

Laboratory experiments were conducted in a flume that was 0.9 m-wide, 14 m-long, and 0.6 m-deep in the Iran University of Science and Technology. The flow rate (31.7 L/s) was measured by an electromagnetic flow meter installed at the entrance of the flume. The water depth of 44 cm upstream of the pool was controlled by adjusting the tailgate located at the end of the flume. The entrance section of the pool was 6 m long, which was sufficient to ensure the uniform flow of the upstream of the pool. As shown in Figure 3a, to simulate submerged vegetation, many rigid plastic cylindrical elements, with a diameter (D) and mean height (\bar{h}_p) of 10 mm and 12.14 cm, respectively, were placed in a bed with an irregular array. Three area densities of vegetation were used, namely, $\varnothing = 2.3 \times 10^{-3}$, 4.7×10^{-3} , and 7×10^{-3} , (Figure 3e–g), where $\varnothing = A_r \pi D^2 / 4$ is defined as the area density of vegetation and $A_r = N / (L_{veg} \times B_{veg})$, N is the total number of vegetation elements, and $L_{veg} = 2.4$ m and $B_{veg} = 0.6$ m are the length and width of the vegetated area along with the streamwise and spanwise directions, respectively. Additionally, the measurements were conducted in the bare pool (without vegetation) to compare results with the presence of vegetation to those without vegetation in the pool.

As shown in Figure 3a, the vegetation elements were placed on one 20-mm thick wooden board with holes to facilitate variation in the area density (\varnothing). The entrance and exit slopes of the pool were determined using prefabricated wooden templates (Figure 3a). The bed topography of the pool was surveyed using the tool shown in Figure 3c. This tool consists of a ruler and a thin wooden rod, glued to the end of the ruler that can be moved up and down; the heights of the bed at different points were then measured. The bed topography was drawn by transferring data collected to the Surfer software (Figure 3h).

The pool inlet flows depth H and flow rate Q were kept constant for each designated area density of vegetation. Since the pool inlet flows depth changes from the upstream to the downstream, the Relative Submergence H/\bar{h}_p changed with a range of 3.55 to 4.60. The variable's \varnothing values were selected to create different flow conditions, as shown in Table 1.

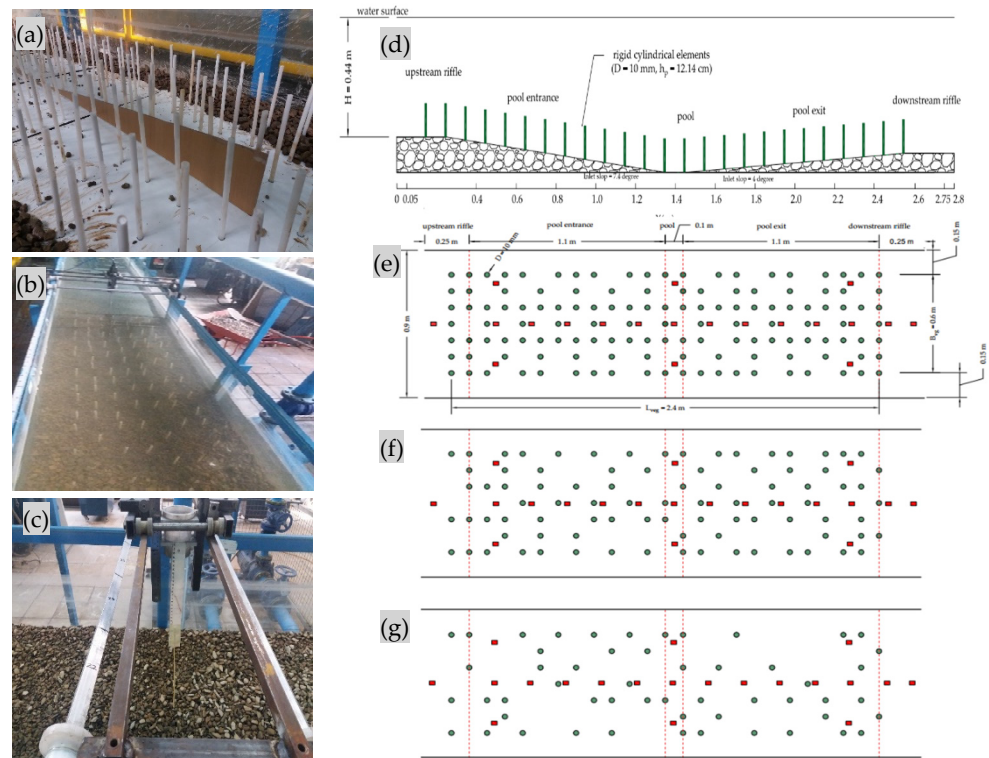


Figure 3. Cont.

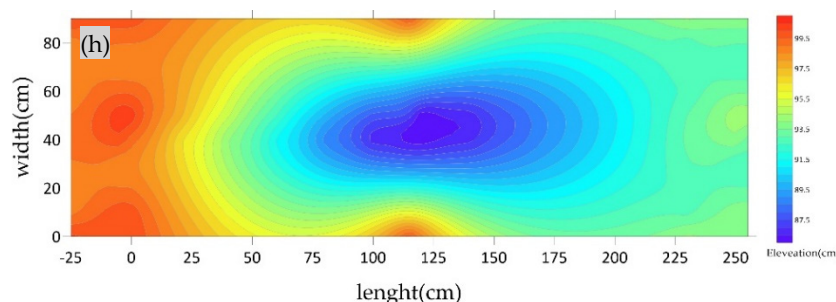


Figure 3. Laboratory set up. (a) The vegetation elements and prefabricated wooden templates, (b) instantaneous velocity measurements using an ADV, (c) the tool for topographical bed survey, (d) side view of the riffle-pool-riffle bedform, (e) the irregular array pattern of vegetation elements with $\varnothing = 7 \times 10^{-3}$, (f) $\varnothing = 4.7 \times 10^{-3}$, (g) $\varnothing = 2.3 \times 10^{-3}$, and (h) bed topographic contours. Note: the green-color circles are vegetated elements and red-color rectangles represent the location of the velocity measurements.

Table 1. Experimental conditions.

Case	Vegetation Density \varnothing	Q (L/s)	Bedform Amplitude Δ (m)	Ratio Δ/λ
I	7×10^{-3}	31.7 ± 0.1	0.1428	0.051
II	4.7×10^{-3}	31.7 ± 0.1	0.1428	0.051
III	2.3×10^{-3}	31.7 ± 0.1	0.1428	0.051
IV	bare pool	31.7 ± 0.1	0.1428	0.051

The pool-riffle morphology in the study river reach was used in this study to represent a dominant bedform in gravel-bed rivers, as described in Section 2.1. Accordingly, an artificial pool was then constructed in the laboratory in a straight flume. The wavelength λ and amplitude Δ of the pool-riffle topography depends on the flow rate [43], the grain size of bed material, particle grading [44], and the presence of externally imposed flow obstructions such as wood, bedrock outcrops, etc. [45]. In the present study, experiments were carried out in a straight riffle-pool-riffle channel without any obstructions. The channel bed was covered with vegetation elements by considering different area densities of vegetation. In natural gravel-bed rivers, the self-formed pool-riffle channels typically have a mean pool wavelength λ of about five to seven times the bank-full widths [46], although it may be as low as three times the channel widths [47]. The pool-riffle amplitude (Δ) was determined by the residual pool depth, which was defined as the difference in elevation between the riffle crest and the pool bottom [48]. With a constant bedform wavelength (2.8 m), the ratio of the pool amplitude to the wavelength, Δ/λ , had the value of 0.051 in this study. The gravel particle size of bed material used in the experiments ranged from 5 to 50 mm, with a median grain size of $d_{50} = 23.3$ mm, $d_{i6} = 14$ mm, and $d_{84} = 40$ mm (Figure 2). However, since the geometric standard deviation ($\sigma_g = (d_{84}/d_{16})^{0.5} = 1.69 > 1.4$), the gravel bed materials are not uniformly graded in bed flume. As described in Section 2.1 (Figure 3d), the entrance and exit slopes were 7.4 and 4 degrees, respectively.

A down-looking acoustic Doppler velocimeter (ADV), developed by Nortek, was used to measure the instantaneous three-dimensional velocity components. The first point of measurement was set at a distance of 4 mm from the bed. The Origin package for data processing prepared by Nortek was used to filter and process velocity and turbulence data. However, data with an average correlation coefficient of less than 70% and average SNR of less than 15 dB was filtered out. Each velocity profile was developed based on the mean velocity measured at 23 to 33 points from the point located at 4 mm above the bed to the point located at 5 cm below the water surface. In addition, velocity measurements were made at 14 cross-sections along the riffle-pool-riffle channel from the cross-section 20 cm upstream to the cross-section 20 cm downstream of this channel. It should be noted that due to so many measured velocity data, all analyses were performed in control sections for each Case at the upstream section of the pool ($X/\lambda = 0.017$), the pool entrance ($X/\lambda = 0.21$),

the middle of the pool ($X/\lambda = 0.5$), the pool exit ($X/\lambda = 0.78$), and the downstream section of the pool ($X/\lambda = 0.98$).

3. Theory

3.1. Statistical Description of Velocity

In the inner layer, the streamwise velocity followed the law of the wall, written as the following equation,

$$\frac{u}{u^*} = \frac{1}{\kappa} \ln\left(\frac{z}{z_0}\right) \quad (1)$$

where z is the height above the reference bed level (z_0), u^* is the shear velocity, and κ is the Von Karman coefficient ($\kappa = 0.4$ in uniform flow). Additionally, z_0 was $0.2d_{50}$ in this study. The inner layer has been found to extend to a relative depth of $z/H = 0.2$ in uniform and nonuniform flow [49], but the upper layer is variable [50]. Bed shear stress is a critical parameter for the prediction of sediment transport. Although sediment transport is not within the aim of this paper, it is crucial to qualify the spatial variability of shear stress as a means of assessing the effect of the redistribution of flow and turbulence on the channel boundary. Typical formulae to estimate shear stress from velocity measurements use either the gradient of mean velocity near the bed or some measure of turbulence such as the Reynolds stress or turbulent kinetic energy. Shear velocity is the most fundamental scale with which to normalize mean velocity. However, since its measurement is not trivial, several methods have been proposed to estimate this parameter [51]. Following previous studies of non-uniform flows [52,53] the wake parameter (Π) was determined at each measurement location from a fit of the velocity profile to the wake law [54] following the relation:

$$\frac{u_c - \bar{u}}{u^*} = \frac{1}{\kappa} \ln\left(\frac{z}{z_0}\right) + \frac{2\Pi}{\kappa} \sin^2\left(\frac{\pi}{2} \frac{z}{z_c}\right) \quad (2)$$

where u_c is the maximum velocity in the profile, and z_c is the height above the bed at which the maximum velocity occurs. Relatively high inertia in the outer zone during decelerating flow means that Π will be greater than zero, whereas relatively low inertia in the outer zone during acceleration flow means that Π will be less than zero [55].

3.2. Shear Velocity (Friction Velocity)

In this paper, three estimates of shear velocity (u^*) were calculated to describe the spatial variability. A first estimate of the shear velocity (u^*_{Lw}) was made from the velocity gradient in the inner layer (Equation (1)). The Reynolds stress at the bed τ_{RS} was estimated at the bed reference level z_0 from the Equation (3) in the inner layer to give a second estimate of the shear velocity (u^*_{RS}) with the following Equation,

$$\tau_{RS} = -\overline{\rho u'w'} \rightarrow u^*_{RS} = \sqrt{\frac{\tau_{RS}}{\rho}} \quad (3)$$

where $\rho = 997 \text{ kg/m}^3$ is the fluid density at $25 \text{ }^\circ\text{C}$. This method is sensitive to measurement errors due to the sometimes steep gradients in Reynolds stress in nonuniform flow at the bed [38,53]. A third estimate of the shear velocity (u^*_{TKE}) was calculated from turbulent kinetic energy (Equation (4)):

$$\tau_{TKE} = 0.5c_2\rho \left[\overline{u'^2} + \overline{v'^2} + \overline{w'^2} \right] \rightarrow u^*_{TKE} = \sqrt{\frac{\tau_{TKE}}{\rho}} \quad (4)$$

where c_2 is a constant with a value of approximately 0.19 [56]. This method has been recommended in complex flows because it fails to assume a particular shape for the velocity profile or correlation in turbulent fluctuations [57]. The temporal velocity fluctuation (u' , v' , w') refer to (x , y , z) directions, where x , y , and z are the streamwise, spanwise, and vertical direction in a cartesian coordinate, respectively.

4. Results and Discussion

4.1. Streamwise Velocity and Shear Velocity along the Channel Centerline

The distribution of velocity changes as a result of pool geometry, in which the flow becomes decelerated along the entrance section and accelerated along the exit section, as well as the presence of an irregular pattern of vegetated patches with different area densities, as shown in Figure 4. For all experiment runs, the streamwise velocity u increased considerably near the channel bed ($0 < z < 15$ mm) as the distance from the bed increased, as shown in Table 1. During the deceleration flow (DF), the average streamwise velocity \bar{u} decreased as the area density of vegetation \varnothing decreased, such that the minimum of the \bar{u} occurred when the area density \varnothing was the least (Case IV). In the middle of the pool ($X/\lambda = 0.5$), when the area density \varnothing was the least (Case IV), the average streamwise velocity \bar{u} initially decreased and then increased. On the other hand, \bar{u} decreased with the decrease in area density of vegetation during the acceleration flow (AF). However, the maximum value of \bar{u} was observed when the area density \varnothing was the least (Case IV). As shown by velocity profiles, velocity increased sharply above the vegetated elements (approximately $z > 120$ mm, z represents the distance above the channel bed) at $X/\lambda = 0.5$ for vegetated Case I and at $X/\lambda = 0.5$ and at $X/\lambda = 0.78$ for vegetated Case III. However, for flow between vegetated stems, velocity was small. The streamwise velocity u around the top of vegetated elements was greater than that of the flow between the vegetated stems, implying intensive stress at the top of vegetation (Figure 4(c-i,d-i,e-i)). Kironoto and Graf (1995) pointed out that for an aspect ratio (the ratio of the channel width to the depth of water) of less than 5, the maximum flow velocity occurs under the water surface in AF [49]. In this study, for vegetated Cases I and II, the maximum flow velocity occurred at a depth of $z/H = 0.65$, but for vegetated Case III, it occurred near the water surface in the DF. However, the maximum velocity in the DF in the channel without the presence of vegetation (Case IV) occurred at a depth of $z/H = 0.3$. In contrast, in AF for vegetated Cases II, III, and VI, the maximum velocity occurred near the water surface and occurred at the depth of $z/H = 0.3$ for vegetated Case I. For vegetated Case I, the shear velocity estimated by the law of the wall in the inner layer increased in the DF and decreased as the flow depth decreased in the AF (Figure 5a). This may be considered a misleading result because the near-bed velocity is greater in the AF than that in the DF (Figure 4(b-i,b-j,d-i,d-j)), showing the difference in the shear stress distribution for these flows (AF and DF). Although sediment transport is not within the aim of this study, it is crucial to qualify the spatial variability of shear stress which is used as a means for assessing the effect of the redistribution of flow and turbulence on the channel boundary. Various methods can be used to estimate the shear velocity (u^*) in flows without vegetation in the channel bed [50,58,59] and with vegetation in the channel bed [60]. In this paper, three methods for determining shear velocity were used: the Law of the Wall (u^*_{LW}), the Reynolds stress method (u^*_{RS}), and turbulent kinetic energy (u^*_{TKE}), described in Section 3.2. However, these methods are not appropriate to be applied for flow with vegetation in a channel bed; one important reason is that the stress acting on the bed is only a fraction of the total flow resistance [57,61]. Results of the estimation of shear velocity by the Reynolds stress method (u^*_{RS}) and TKE (u^*_{TKE}) showed that no change was observed along the longitudinal direction of the flow in the vegetated Cases II and III (Figure 5b,c). For Cases I and IV, the minimum shear velocities estimated from the law of the wall in the inner layer were observed at the end of the AF section, instead of in the middle of the pool as it was expected. However, the minimum shear velocities for vegetated Cases II and III occurred in the DF section. At a given flow depth, u^*_{LW} is thus greater in the DF section than that in the AF section, which is not in agreement with results in the pool without vegetation reported by Kironoto et al. [49]. Thus, the location of the minimum u^*_{LW} is not only a function of the flow depth and bed particle size, but the irregular pattern of vegetated elements in the channel bed can also change the location of this value. According to Figure 5d, by comparing the maximum values of the Coles wake parameter (Π) in all Cases, it is found that the $\Pi_{max} = 2$ (for Case I) is larger than that of reported studies in open channels (e.g., $\Pi_{max} = 0.41$ in gravel-bed [49], $\Pi_{max} = 1.35$ [62], and $\Pi_{max} = 0.19$ [63]). This large value for the wake parameter is reasonable. Normally,

higher values for the Coles wake parameter have been observed in wind tunnel experiments with larger pressure gradients (e.g., $\Pi_{max} = 6.9$ in a boundary layer close to the separation zone by Krogstad and Skare (1995) [64] and the flow redistribution in a straight artificial pool (e.g., $\Pi_{max} = 4$ [55]). The wake parameter Π value is positive from the upstream portion of the pool to the downstream of the pool regardless of whether the channel bed of the pool is vegetated or not, indicating that the velocity distributions continue to carry the inertial effects from the upstream of the pool into the downstream portion of the pool. Downstream of the pool ($X/\lambda = 0.92$), the estimated Π value increased again, indicating that the flow is barely recovering toward uniform flow due to the presence of an irregular distribution pattern of vegetated elements for Cases I to III, and due to the variation of bedform in the riffle-pool-riffle for Case IV. However, the minimum of the wake parameter with a negative value of $\Pi = -0.8$ occurring at the downstream limit of the pool has been observed [52]. As shown in Figure 5, for all Cases except Case II in the AF section, the values of u^*_{TKE} are generally less than the values of u^*_{LW} and u^*_{RS} , even if the uniform flow reaches upstream of the pool, implying that the shear velocities calculated by these methods are different, confirming findings of some previous studies [50,65]. In the outer zone, the inertial effects of the flow changed the streamwise velocity profile such that Π increased in the DF section and decreased through the middle of the pool and in the AF section. It also, it increased in the uniform depth section downstream of the pool (Figure 5d).

4.2. The Reynolds Stress along the Channel Centerline

The Reynolds stress $-\overline{u'w'}$ is the most important parameter for estimating the shear stress in a channel bed and investigating the effects of vegetation over the bedform. As shown in Figure 6, similar to the streamwise velocity, the shape of the Reynolds stress $-\overline{u'w'}$ profiles in the pool deviated from the shape of the $-\overline{u'w'}$ profiles in the uniform flow ($X/\lambda = 0.017$, upstream of the pool) due to the AF and DF as well as the presence of an irregular distribution pattern of vegetated elements in channel bed for all Cases. Figure 6 shows the Reynolds stress distribution for all Cases. In the upstream section of the pool (Figure 6a) the flow is normal (e.g., $X/\lambda = 0.5$) and $-\overline{u'w'}$ shows an irregular pattern which is due to a complex interaction of the flow and submerged vegetation. For all Cases, the Reynolds stresses also changed significantly near the bed due to a complex interaction of bedform and an irregular vegetation patch on the bed. Upstream of the pool, very close to the channel bed, the Reynolds stress $-\overline{u'w'}$ decreased toward the bed within a layer approximately 1.3 cm thick. This trend indicates that the bed may not have been utterly flat in the upstream section of the pool. For all Cases inside of the pool, the maximum $-\overline{u'w'}$ occurs at a larger distance above the bed surface depending on the area density of vegetation. For instance, for vegetated Case I, the maximum $-\overline{u'w'}$ occurred at a distance of about 16 cm from the bed, and for vegetated Case III, at a distance of about 19 cm (Figure 6(c-i,c-j)). This effect normally occurs in the DF section (Figure 6(b-i,b-j)) and the AF section (Figure 6(d-i,d-j)) due to the positive and negative streamwise pressure gradients, respectively. In the downstream section of the pool (Figure 6(e-i,e-j)), the distribution of $-\overline{u'w'}$ is different from the distribution observed in the upstream section of the pool due to severe perturbations caused by bedform and the irregular pattern of submerged vegetated elements. The $-\overline{u'w'}$ at some cross-sections (e.g., $X/\lambda = 0.78$ and $X/\lambda = 0.98$) had increased significantly, especially for Case I (Figure 6(d-i,e-i)). It could be explained by flow velocities inducing strong fluctuations in the channel when they met the vegetated elements, especially in these two different zones. In a rectangular channel, the Reynolds stress $-\overline{u'w'}$ can be negative due to a velocity dip caused by secondary currents [66]. A negative Reynolds stress $-\overline{u'w'}$ indicates an upward vertical transport of momentum with negative velocity gradients. Furthermore, negative values of $-\overline{u'w'}$ in zones with positive velocity gradients may occur due to the transfer of turbulent energy from some localized zones to the mean flow [67]. In this study, due to the resistance resulting from vegetation elements, negative values of $-\overline{u'w'}$ can also be observed close to the edge of the vegetation patch (e.g., Figure 6(d-j,e-i,e-j)). However, the irregular fluctuations of stresses are due to a

complex flow field caused by the pool and submerged vegetation elements which cannot be easily explained by the momentum equation.

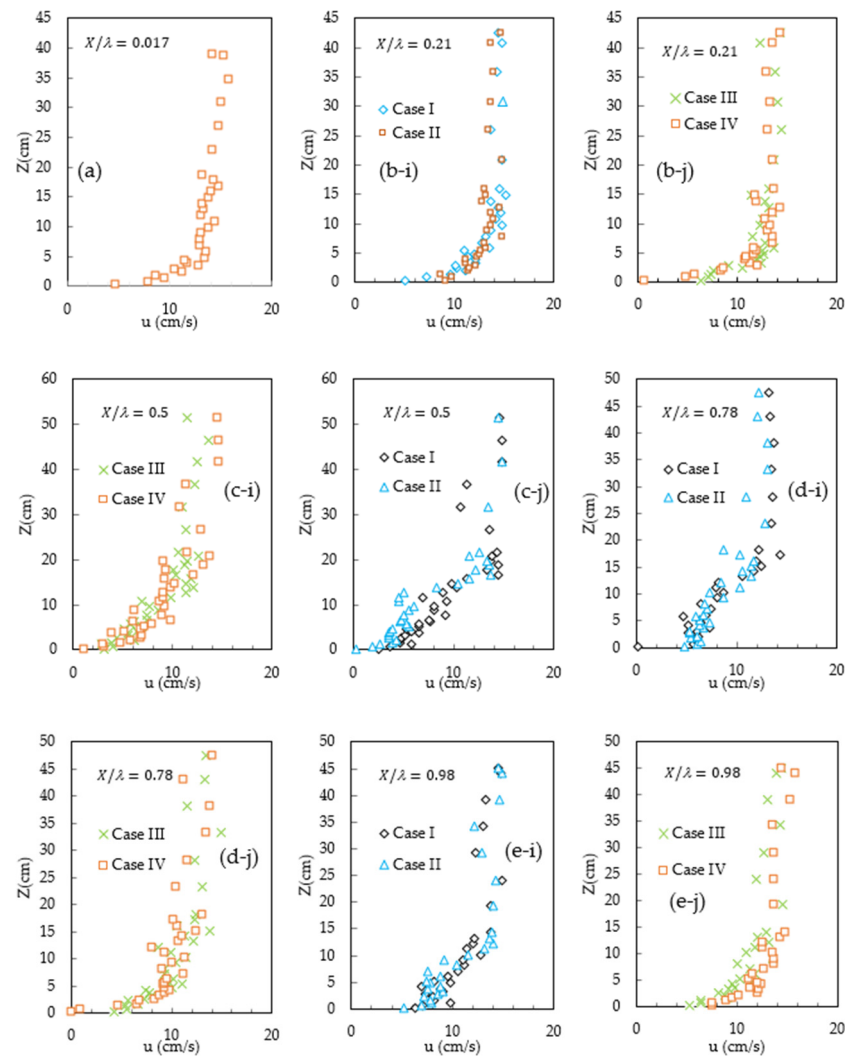


Figure 4. Profiles of streamwise velocity along the channel centerline for all Cases. (a) The upstream section of the pool ($X/\lambda = 0.017$, (b-i,b-j) the pool entrance ($X/\lambda = 0.21$), (c-i,c-j) the middle of the pool ($X/\lambda = 0.5$), (d-i,d-j) the pool exit ($X/\lambda = 0.78$), and (e-i,e-j) the downstream section of the pool ($X/\lambda = 0.98$).

4.3. Turbulence Kinetic Energy

To examine zones for the turbulence production and dissipation, the flow of turbulent energy can be determined by calculating the Turbulent Kinetic Energy ($TKE = 0.5 \rho [u'^2 + v'^2 + w'^2]$), where ρ is the density of water and u'^2 , v'^2 , and w'^2 are the mean square values of the fluctuations in velocity in the streamwise, lateral, and vertical directions, respectively. As shown in Figure 7, the TKE value is presented against the water depth z . The turbulent kinetic energy profile upstream of the pool (Figure 7a at $X/\lambda = 0.017$) shows approximately the same pattern as that for the Reynolds stress in Figure 6a. For all Cases in the DF section, the TKE decreases with the water depth z and its maximum appears approximately at the channel bed. However, for vegetated Case I, the TKE attains its peak at both the channel bed and a certain distance above the bed ($z \cong 1$ cm). Similarly, for Case III, the TKE attains its peak at a distance from the bed of $z \cong 2.5$ cm from the bed, however, the maximum TKE for Case IV (bare bed) is smaller than that for Case III (Figure 7(b-i,b-j)). For Cases I and

IV (Figure 7(b-i,b-j)) near the bed, the TKE reached its maximum value, indicating that the turbulence generated by the irregular pattern of vegetated elements in the bed plays a key role in the vertical distribution of the TKE. Inside the pool (Figure 7(c-i,c-j)), the maximum TKE occurs at a larger distance from the bed surface, depending on the area density of vegetation. The momentum exchange and turbulent energy are likely influenced by the secondary circulations associated with the irregular distribution of vegetated elements in the channel bed. However, as the area density decreases, the maximum TKE decreases in the AF section, indicating the influence of the AF pool and the submerged vegetation. Downstream of the pool ($X/\lambda = 0.98$), the TKE profile shows a similar pattern as that observed upstream of the pool (Figure 7(e-i,e-j)). The TKE values indicate irregular distribution near the vegetated elements. However, with an increase in the distance from the bed, the irregular distribution reduces (Figure 7(d-i)).

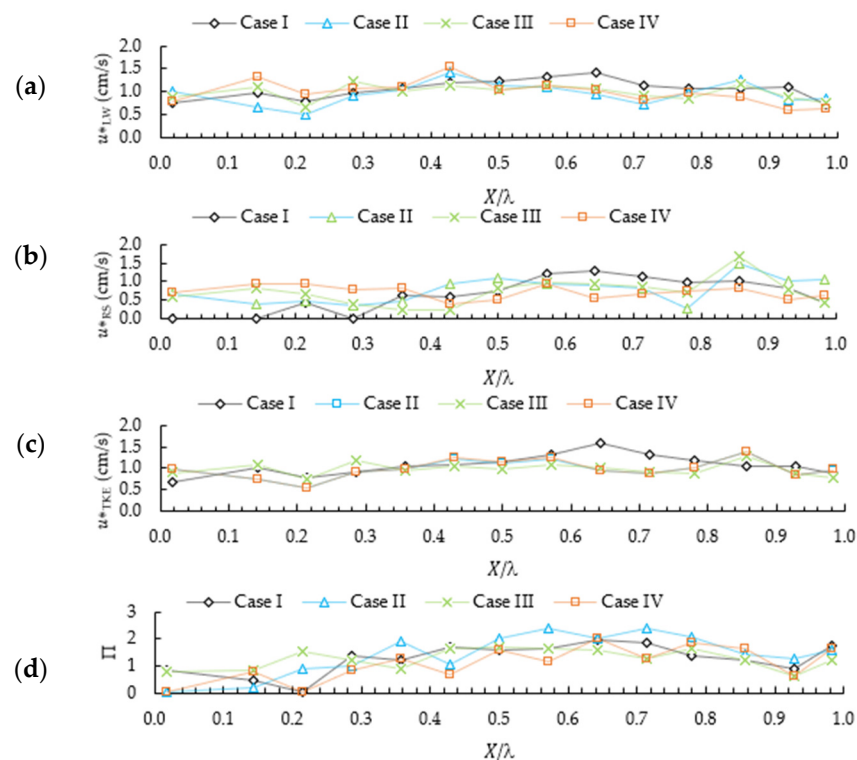


Figure 5. (a) Shear velocity according to the law of wall (u^*_{Lw}), (b) shear velocity according to the Reynolds stress (u^*_{RS}), (c) shear velocity according to the turbulent kinetic energy (u^*_{TKE}), and (d) Coles wake parameter (Π) along the channel centerline from upstream to downstream of the bedform.

The differences in TKE values at a certain flow depth might be caused by positive and negative streamwise pressure gradients and irregular patterns of vegetated elements in the AF and DF sections, respectively. These results were similar to those observed by Sukhodolov (2012), where the bias of the TKE profile indicated the cumulative effect of mixing and boundary layers generated by the area density of vegetation [68].

4.4. Quadrant Analysis

In this paper, a quadrant analysis was performed using a bursting cycle detection method [67], as shown in Figure 8. Two quadrants (Q_{ej} and Q_{sw}) contribute positively and the other two quadrants (Q_{out} interactions and Q_{inw} interactions) contribute negatively to the overall principal Reynolds stresses. To determine the contribution of each quadrant to the shear events, a computer program was written in MATLAB. Figure 8 shows the results of the quadrant analysis in the presence of irregular vegetation patterns for all Cases from the upstream section of the pool (Figure 8a at $X/\lambda = 0.017$), the pool entrance (Figure 8b

at $X/\lambda = 0.21$), the middle of the pool (Figure 8c at $X/\lambda = 0.5$), the pool exit (Figure 8d at $X/\lambda = 0.78$) and the downstream section of the pool (Figure 8e at $X/\lambda = 0.98$), respectively. A quadrant analysis using the bursting cycle detection method at points of specified height, at the entire depth of the flow, was performed from the upstream section of the pool to the downstream of the pool for all Cases. For Case IV, results showed that ejections are dominant the upstream of the pool ($X/\lambda = 0.5$) at a distance of about 4 cm from the bed, as expected from the boundary layer development in a uniform flow [54], and the sweeps are stronger at a distance between 4 cm to 11 cm from the bed. Near the water surface, the velocity is higher. Thus, toward the water surface, the outward event tends to grow and reach the highest value. In the FD section ($X/\lambda = 0.21$), ejections are dominant near the bed while sweeps are stronger near the water surface for all Cases. With the presence of the irregular distribution of vegetated elements in the channel bed of the pool ($X/\lambda = 0.5$), ejections become dominant (for Case I, II, and III) and then the outward event becomes stronger as the area density of vegetation decreases (for Cases IV).

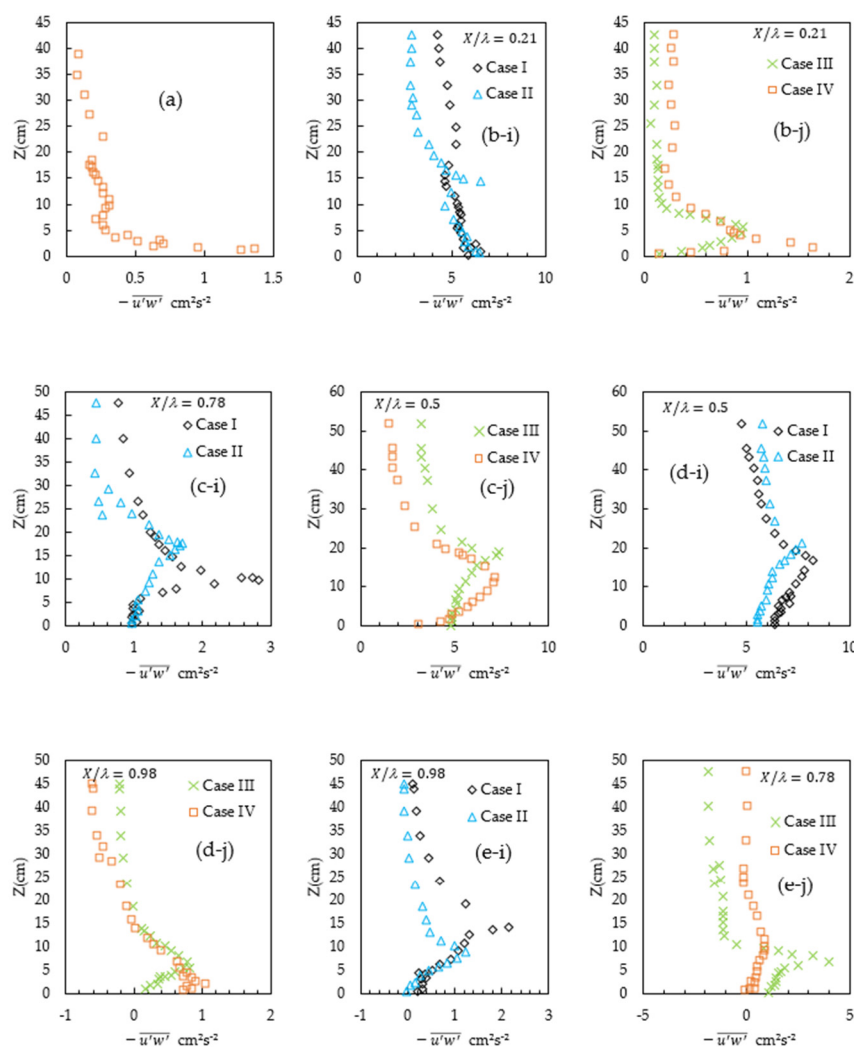


Figure 6. Profiles of the Reynolds stress $-\overline{u'w'}$ along the channel centerline for all Cases. (a) The upstream section of the pool ($X/\lambda = 0.017$), (b-i,b-j) the pool entrance ($X/\lambda = 0.21$), (c-i,c-j) the middle of the pool ($X/\lambda = 0.5$), (d-i,d-j) the pool exit ($X/\lambda = 0.78$), and (e-i,e-j) the downstream section of the pool ($X/\lambda = 0.98$).

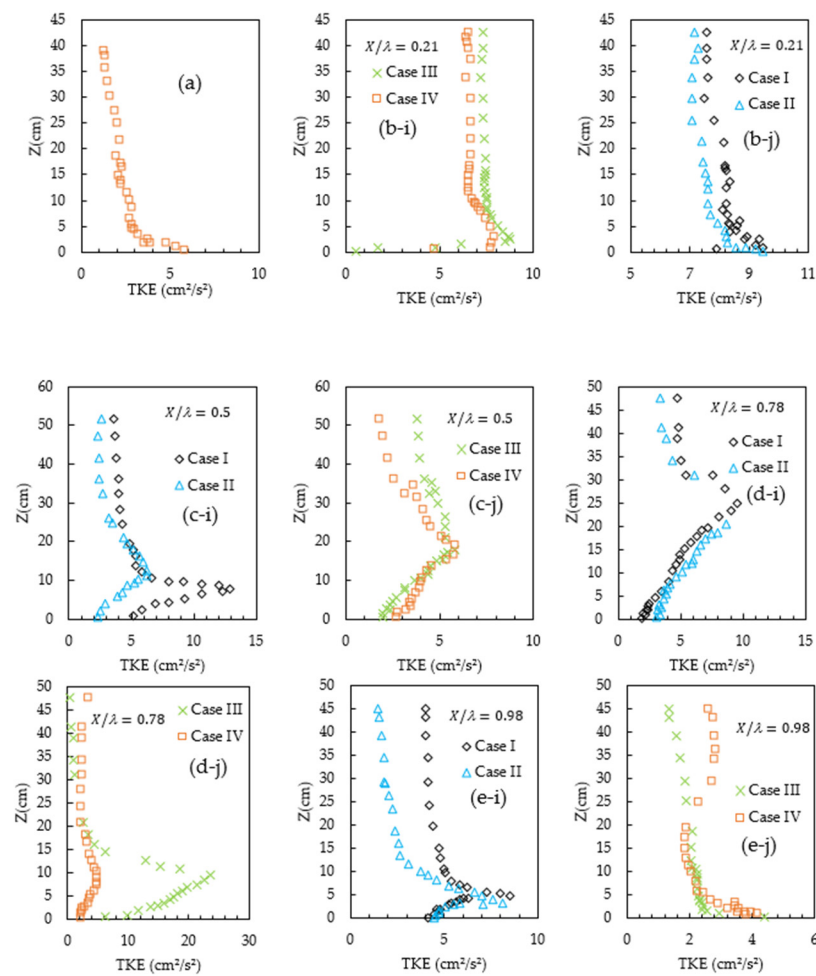


Figure 7. Profiles of the TKE values along the channel centerline for all Cases. (a) The upstream section of the pool ($X/\lambda = 0.017$), (b-i,b-j) the pool entrance ($X/\lambda = 0.21$), (c-i,c-j) the middle of the pool ($X/\lambda = 0.5$), (d-i,d-j) the pool exit ($X/\lambda = 0.78$), and (e-i,e-j) the downstream section of the pool ($X/\lambda = 0.98$).

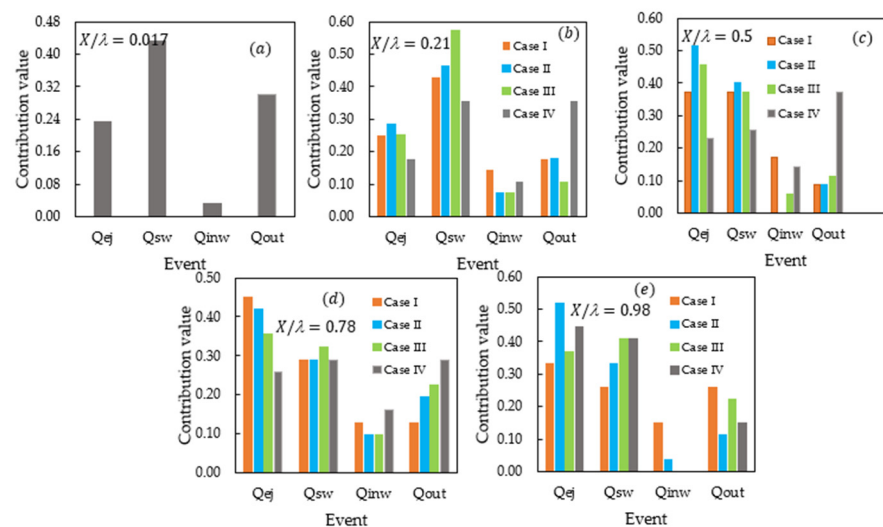


Figure 8. Quadrant analysis using the bursting cycle detection method at (a) the upstream section of the pool ($X/\lambda = 0.017$), (b) the pool entrance ($X/\lambda = 0.21$), (c) the middle of the pool ($X/\lambda = 0.5$), (d) the pool exit ($X/\lambda = 0.78$), and (e) the downstream section of the pool ($X/\lambda = 0.98$) for all Cases.

Within the AF section ($X/\lambda = 0.78$), sweeps are again dominant for Case IV and ejections for Cases I, II, and III. In the downstream section of the pool ($X/\lambda = 0.98$), for all Cases, ejections and sweeps are dominant. However, in the presence of an irregular pattern of vegetated elements in the pool, both the ejections and sweeps are stronger events than both inward and outward events.

5. Conclusions

In this paper, the turbulent flow field has been studied based on laboratory experiments with the presence of submerged rigid vegetation elements in the channel bed of a straight pool with different entry and exit slopes. Considering the distribution profiles of velocity, shear stress, turbulence kinetic energy, and quadrant analysis, the following results have been drawn from this study:

- The variations in velocity along the pool section with the submerged vegetation in the channel bed are different from that in the bare pool. In the entrance section of the pool where the flow is decelerating, a regular velocity distribution pattern is observed without any reversal flow even though the pressure gradient is unfavorable. However, in the exit section of the pool where the flow is accelerating and the pressure gradient is favorable, a reverse flow near the bed is observed. This is due to the appearance of a positive pressure gradient developed in this section. This difference in velocity pattern shows the influence of the submerged vegetation on the velocity distribution.
- A suitable method for estimating the shear velocity for the flow with the presence of submerged vegetation in the channel bed is the TKE method (u^*_{TKE}), since all the fluctuation components of turbulence have been used in this method. In fact, the strong lateral component of turbulence fluctuation v'^2 does not appear in the Reynolds stress method. In addition, when the area density of vegetation decreases, the location of the maximum u^*_{TKE} changes along with the pool.
- The shape and the location of the maximum value of the Reynolds stress distribution depend on the slopes of the entrance and the exit section of the pool. In addition, the distribution pattern of vegetated elements in the channel bed also affects the shape and the location of the maximum value of the Reynolds stress distribution. In general, the Reynolds stress distribution in the pool with the presence of vegetation in the bed is irregular and is considerably different from that in the bare pool.
- For all investigated Cases within the pool, the maximum Reynolds stress and TKE occur at a larger distance above the bed surface, depending on the area density of vegetation. The irregular distributions of Reynolds stress and TKE result from the secondary circulations associated with the irregular distribution pattern of vegetated elements in the channel bed.
- Results of the quadrant analysis show that the momentum between flow, bedform and vegetated elements are mostly transferred by sweep and ejection events. Toward the water surface, the outward event becomes the dominant event. At the pool entrance where the flow is decelerating, the ejection event is dominant near the bed while the sweep event is strong near the water surface. In the presence of an irregular distribution of submerged vegetated elements in the pool-bed, ejections become dominant (for Case I, II, and III) and then the outward event becomes stronger as the area density of vegetation decreases (for Cases IV).

Author Contributions: K.N., field works, methodology, software, writing—original draft, preparation; H.A., supervision, writing—review, methodology, validation and editing; J.S., methodology, writing—review and editing. All authors have read and agreed to the published version of the manuscript.

Funding: This research received no external funding.

Institutional Review Board Statement: Not applicable.

Informed Consent Statement: Not applicable.

Data Availability Statement: Data are contained within the article.

Acknowledgments: The authors would like to acknowledge that Ruhollah Nouri Pour, a water engineering graduate from Shiraz University in Iran, helped with the topographic survey of natural rivers.

Conflicts of Interest: The authors declare no conflict of interest.

References

1. Wilcock, R.J.; Nagels, J.W.; Rodda, H.J.; O'Connor, M.B.; Thorrold, B.S.; Barnett, J.W. Water quality of a lowland stream in a New Zealand dairy farming catchment. *N. Z. J. Mar. Freshw. Res.* **1999**, *33*, 683–696. [[CrossRef](#)]
2. Yamasaki, T.N.; Jiang, B.; Janzen, J.G.; Nepf, H.M. Feedback between vegetation, flow, and deposition: A study of artificial vegetation patch development. *J. Hydrol.* **2021**, *598*, 126232. [[CrossRef](#)]
3. Beltrão, G.d.B.M.; Medeiros, E.S.F.; Ramos, R.T.d.C. Effects of riparian vegetation on the structure of the marginal aquatic habitat and the associated fish assemblage in a tropical Brazilian reservoir. *Biota Neotrop.* **2009**, *9*, 37–43. [[CrossRef](#)]
4. Schoelynck, J.; De Groot, T.; Bal, K.; Vandenbruwaene, W.; Meire, P.; Temmerman, S. Self-organised patchiness and scale-dependent bio-geomorphic feedbacks in aquatic river vegetation. *Ecography* **2012**, *35*, 760–768. [[CrossRef](#)]
5. Nosrati, K.; Afzalimehr, H.; Sui, J. Drag Coefficient of Submerged Flexible Vegetation Patches in Gravel Bed Rivers. *Water* **2022**, *14*, 743. [[CrossRef](#)]
6. Nasiri Dehsorkhi, E.; Afzalimehr, H.; Singh, V.P. Effect of bed forms and vegetated banks on velocity distributions and turbulent flow structure. *J. Hydrol. Eng.* **2011**, *16*, 495–507. [[CrossRef](#)]
7. Nepf, H.M. Hydrodynamics of vegetated channels. *J. Hydraul. Res.* **2012**, *50*, 262–279. [[CrossRef](#)]
8. Nepf, H.M.; Vivoni, E. Flow structure in depth-limited, vegetated flow. *J. Geophys. Res. Ocean.* **2000**, *105*, 28547–28557. [[CrossRef](#)]
9. Kazem, M.; Afzalimehr, H.; Sui, J. Formation of Coherent Flow Structures beyond Vegetation Patches in Channel. *Water* **2021**, *13*, 2812. [[CrossRef](#)]
10. Gambi, M.C.; Nowell, A.R.; Jumars, P.A. Flume observations on flow dynamics in *Zostera marina* (eelgrass) beds. *Mar. Ecol. Prog. Ser.* **1990**, *61*, 159–169. [[CrossRef](#)]
11. Nepf, H.; Vivoni, E. Turbulence structure in depth-limited vegetated flow: Transition between emergent and submerged regimes. In Proceedings of the 28th International IAHR Conference, Graz, Austria, 22–27 August 1999.
12. Afzalimehr, H.; Subhasish, D. Influence of bank vegetation and gravel bed on velocity and Reynolds stress distributions. *Int. J. Sediment Res.* **2009**, *24*, 236–246. [[CrossRef](#)]
13. Baptist, M.J. A flume experiment on sediment transport with flexible, submerged vegetation. In Proceedings of the International Workshop on Riparian Forest Vegetated Channels: Hydraulic, Morphological and Ecological Aspects, RIPFOR, Trento, Italy, 20–22 February 2003.
14. Afzalimehr, H.; Barahimi, M.; Sui, J. Non-uniform flow over cobble bed with submerged vegetation strip. In Proceedings of the Institution of Civil Engineers-Water Management; Thomas Telford Ltd.: London, UK, 2019; Volume 172, pp. 86–101.
15. Ackerman, J.; Okubo, A. Reduced mixing in a marine macrophyte canopy. *Funct. Ecol.* **1993**, *7*, 305–309. [[CrossRef](#)]
16. Lynn, A.L.; Reed, D.J. Hydrodynamics and sediment transport through tidal marsh canopies. *J. Coast. Res.* **2002**, *36*, 459–469. [[CrossRef](#)]
17. Klopstra, D.; Barneveld, H.; Van Noortwijk, J.; Van Velzen, E. Analytical model for hydraulic roughness of submerged vegetation. In Proceedings of Theme A, Managing Water: Coping with Scarcity and Abundance, Proceedings of the 27th Congress of the International Association for Hydraulic Research, San Francisco, CA, USA, 10–15 August 1997; American Society of Civil Engineers (ASCE): New York, NY, USA, 1997; pp. 775–780.
18. Jahadi, M.; Afzalimehr, H.; Ashrafizaadeh, M.; Kumar, B. A numerical study on hydraulic resistance in flow with vegetation patch. *ISH J. Hydraul. Eng.* **2022**, *28*, 243–250. [[CrossRef](#)]
19. Baptist, M.; Babovic, V.; Rodríguez Uthurburu, J.; Keijzer, M.; Uittenbogaard, R.; Mynett, A.; Verwey, A. On inducing equations for vegetation resistance. *J. Hydraul. Res.* **2007**, *45*, 435–450. [[CrossRef](#)]
20. Liu, D.; Diplas, P.; Fairbanks, J.; Hodges, C. An experimental study of flow through rigid vegetation. *J. Geophys. Res. Earth Surf.* **2008**, *113*. [[CrossRef](#)]
21. Stone, B.M.; Shen, H.T. Hydraulic resistance of flow in channels with cylindrical roughness. *J. Hydraul. Eng.* **2002**, *128*, 500–506. [[CrossRef](#)]
22. Defina, A.; Bixio, A.C. Mean flow and turbulence in vegetated open channel flow. *Water Resour. Res.* **2005**, *41*. [[CrossRef](#)]
23. Yang, W.; Choi, S.-U. A two-layer approach for depth-limited open-channel flows with submerged vegetation. *J. Hydraul. Res.* **2010**, *48*, 466–475. [[CrossRef](#)]
24. Li, S.; Shi, H.; Xiong, Z.; Huai, W.; Cheng, N. New formulation for the effective relative roughness height of open channel flows with submerged vegetation. *Adv. Water Resour.* **2015**, *86*, 46–57. [[CrossRef](#)]
25. Pasquino, V.; Gualtieri, P. Flow resistance of submerged rigid vegetation: Focus and validation on two layer approach. In Proceedings of the 37th IAHR World Congress, Kuala Lumpur, Malaysia, 13–18 October 2017; pp. 13–18.
26. Huthoff, F.; Augustijn, D.C.; Hulscher, S.J. Analytical solution of the depth-averaged flow velocity in case of submerged rigid cylindrical vegetation. *Water Resour. Res.* **2007**, *43*. [[CrossRef](#)]
27. Cheng, N.S. Representative roughness height of submerged vegetation. *Water Resour. Res.* **2011**, *47*. [[CrossRef](#)]

28. Nikora, N.; Nikora, V.; O'Donoghue, T. Velocity profiles in vegetated open-channel flows: Combined effects of multiple mechanisms. *J. Hydraul. Eng.* **2013**, *139*, 1021–1032. [[CrossRef](#)]
29. Nepf, H.; Ghisalberti, M. Flow and transport in channels with submerged vegetation. *Acta Geophys.* **2008**, *56*, 753–777. [[CrossRef](#)]
30. Raupach, M.R.; Finnigan, J.J.; Brunet, Y. Coherent eddies and turbulence in vegetation canopies: The mixing-layer analogy. In *Boundary-Layer Meteorology 25th Anniversary Volume, 1970–1995*; Springer: Berlin/Heidelberg, Germany, 1996; pp. 351–382.
31. Ghisalberti, M.; Nepf, H.M. 3-Mixing layers and coherent structures in vegetated aquatic flows. *J. Geophys. Res.-Part C-Ocean.* **2002**, *107*, 1. [[CrossRef](#)]
32. Nepf, H.M. Flow and transport in regions with aquatic vegetation. *Annu. Rev. Fluid Mech.* **2012**, *44*, 123–142. [[CrossRef](#)]
33. Zhao, H.; Yan, J.; Yuan, S.; Liu, J.; Zheng, J. Effects of submerged vegetation density on turbulent flow characteristics in an open channel. *Water* **2019**, *11*, 2154. [[CrossRef](#)]
34. Rhoads, B.L. Review of River Channels: Environment and Process. *Geogr. Rev.* **1989**, *79*, 119–121. [[CrossRef](#)]
35. Rhoads, B.L.; Welford, M.R. Initiation of river meandering. *Prog. Phys. Geogr.* **1991**, *15*, 127–156. [[CrossRef](#)]
36. Simon, A.; Bennett, S.J.; Castro, J.M. *Stream Restoration in Dynamic Fluvial Systems: Scientific Approaches, Analyses, and Tools*; John Wiley & Sons: Hoboken, NJ, USA, 2013; Volume 194.
37. Yang, S.-Q.; Chow, A.T. Turbulence structures in non-uniform flows. *Adv. Water Resour.* **2008**, *31*, 1344–1351. [[CrossRef](#)]
38. Kabiri, F.; Afzalimehr, H.; Sui, J. Flow structure over a wavy bed with vegetation cover. *Int. J. Sediment Res.* **2017**, *32*, 186–194. [[CrossRef](#)]
39. Afzalimehr, H.; Nosrati, K.; Kazem, M. Resistance to Flow in a Cobble-Gravel Bed River with Irregular Vegetation Patches and Pool-Riffle Bedforms (Case study: Padena Marbor River). *Ferdowsi Civ. Eng. (JFCEI)* **2021**, *2*, 35–50.
40. Chakraborty, P.; Sarkar, A. Flow characteristics through submerged rigid vegetation over a sinusoidal perturbed bed. *Int. J. River Basin Manag.* **2016**, *14*, 255–266. [[CrossRef](#)]
41. Chakraborty, P.; Sarkar, A. Turbulent flow through a random rigid submerged vegetation over a sinusoidal bed. *J. Appl. Water Eng. Res.* **2021**, *9*, 147–160. [[CrossRef](#)]
42. Tubino, M. Growth of alternate bars in unsteady flow. *Water Resour. Res.* **1991**, *27*, 37–52. [[CrossRef](#)]
43. Lanzoni, S.; Tubino, M. Grain sorting and bar instability. *J. Fluid Mech.* **1999**, *393*, 149–174. [[CrossRef](#)]
44. Buffington, J.M.; Lisle, T.E.; Woodsmith, R.D.; Hilton, S. Controls on the size and occurrence of pools in coarse-grained forest rivers. *River Res. Appl.* **2002**, *18*, 507–531. [[CrossRef](#)]
45. Leopold, L.B.; Wolman, M.G.; Miller, J.P.; Wohl, E.; Wohl, E.E. *Fluvial Processes in Geomorphology*; W. H. Freeman & Company: San Francisco, CA, USA, 1964.
46. Carling, P.A.; Orr, H.G. Morphology of riffle–pool sequences in the River Severn, England. *Earth Surf. Processes Landf. J. Br. Geomorphol. Res. Group* **2000**, *25*, 369–384. [[CrossRef](#)]
47. Lisle, T.E.; Hilton, S. The Volume of Fine Sediment in Pools: An Index of Sediment Supply in Gravel-Bed Streams 1. *JAWRA J. Am. Water Resour. Assoc.* **1992**, *28*, 371–383. [[CrossRef](#)]
48. Kironoto, B.; Graf, W.H.; Reynolds. Turbulence characteristics in rough uniform open-channel flow. *Proc. Inst. Civ. Eng.-Water Marit. Energy* **1994**, *106*, 333–344. [[CrossRef](#)]
49. Afzalimehr, H.; Rennie, C.D. Determination of bed shear stress in gravel-bed rivers using boundary-layer parameters. *Hydrol. Sci. J.* **2009**, *54*, 147–159. [[CrossRef](#)]
50. Afzalimehr, H.; Ancil, F. Accelerating shear velocity in gravel-bed channels. *Hydrol. Sci. J.* **2000**, *45*, 113–124. [[CrossRef](#)]
51. Kironoto, B.; Graf, W.H.; Reynolds. Turbulence characteristics in rough non-uniform open-channel flow. *Proc. Inst. Civ. Eng.-Water Marit. Energy* **1995**, *112*, 336–348. [[CrossRef](#)]
52. Song, T.; Chiew, Y. Turbulence measurement in nonuniform open-channel flow using acoustic Doppler velocimeter (ADV). *J. Eng. Mech.* **2001**, *127*, 219–232. [[CrossRef](#)]
53. Coles, D. The law of the wake in the turbulent boundary layer. *J. Fluid Mech.* **1956**, *1*, 191–226. [[CrossRef](#)]
54. MacVicar, B.J.; Rennie, C.D. Flow and turbulence redistribution in a straight artificial pool. *Water Resour. Res.* **2012**, *48*. [[CrossRef](#)]
55. Stapleton, K.; Huntley, D. Seabed stress determinations using the inertial dissipation method and the turbulent kinetic energy method. *Earth Surf. Processes Landf.* **1995**, *20*, 807–815. [[CrossRef](#)]
56. Biron, P.M.; Robson, C.; Lapointe, M.F.; Gaskin, S.J. Comparing different methods of bed shear stress estimates in simple and complex flow fields. *Earth Surf. Processes Landf. J. Br. Geomorphol. Res. Group* **2004**, *29*, 1403–1415. [[CrossRef](#)]
57. Dodaro, G.; Tafarojnoruz, A.; Stefanucci, F.; Adduce, C.; Calomino, F.; Gaudio, R.; Sciortino, G. An experimental and numerical study on the spatial and temporal evolution of a scour hole downstream of a rigid bed. In Proceedings of the International Conference on Fluvial Hydraulics, River Flow, Lausanne, Switzerland, 3–5 September 2014; pp. 3–5.
58. Dodaro, G.; Tafarojnoruz, A.; Sciortino, G.; Adduce, C.; Calomino, F.; Gaudio, R. Modified Einstein sediment transport method to simulate the local scour evolution downstream of a rigid bed. *J. Hydraul. Eng.* **2016**, *142*, 04016041. [[CrossRef](#)]
59. Yang, J.Q.; Kerger, F.; Nepf, H.M. Estimation of the bed shear stress in vegetated and bare channels with smooth beds. *Water Resour. Res.* **2015**, *51*, 3647–3663. [[CrossRef](#)]
60. Rowiński, P.M.; Kubrak, J. A mixing-length model for predicting vertical velocity distribution in flows through emergent vegetation. *Hydrol. Sci. J.* **2002**, *47*, 893–904. [[CrossRef](#)]
61. Onitsuka, K.; Akiyama, J.; Matsuoka, S. Prediction of velocity profiles and Reynolds stress distributions in turbulent open-channel flows with adverse pressure gradient. *J. Hydraul. Res.* **2009**, *47*, 58–65. [[CrossRef](#)]

62. Coleman, H.W.; Moffat, R.J.; Kays, W.M. The accelerated fully rough turbulent boundary layer. *J. Fluid Mech.* **1977**, *82*, 507–528. [[CrossRef](#)]
63. Krogstad, P.Å.; Skåre, P.E. Influence of a strong adverse pressure gradient on the turbulent structure in a boundary layer. *Phys. Fluids* **1995**, *7*, 2014–2024. [[CrossRef](#)]
64. Kim, S.-C.; Friedrichs, C.; Maa, J.-Y.; Wright, L. Estimating bottom stress in tidal boundary layer from acoustic Doppler velocimeter data. *J. Hydraul. Eng.* **2000**, *126*, 399–406. [[CrossRef](#)]
65. Kang, H.; Choi, S.U. Reynolds stress modelling of rectangular open-channel flow. *Int. J. Numer. Methods Fluids* **2006**, *51*, 1319–1334. [[CrossRef](#)]
66. Siniscalchi, F.; Nikora, V.I.; Aberle, J. Plant patch hydrodynamics in streams: Mean flow, turbulence, and drag forces. *Water Resour. Res.* **2012**, *48*. [[CrossRef](#)]
67. Sukhodolov, A.N.; Sukhodolova, T.A. Vegetated mixing layer around a finite-size patch of submerged plants: Part 2. Turbulence statistics and structures. *Water Resour. Res.* **2012**, *48*. [[CrossRef](#)]
68. Willmarth, W.; Lu, S. Structure of the Reynolds stress near the wall. *J. Fluid Mech.* **1972**, *55*, 65–92. [[CrossRef](#)]